ACS APPLIED MATERIALS & INTERFACES

Research Article

Cite This: ACS Appl. Mater. Interfaces XXXX, XXX, XXX−XXX

www.acsami.org

Highly Durable and Flexible Transparent Electrode for Flexible Optoelectronic Applications

Sang Woo Jin,[†,∥] Yong Hui Lee,[‡,∥] Kyung Mun Yeom,[§] Junyeong Yun,[‡] Heun Park,[‡] Yu Ra Jeong,[‡] Soo Yeong Hong,[‡] Geumbee Lee,[†] Seung Yun Oh,[†] Jin Ho Lee,[†] Jun Hong Noh,*[,§,⊥] and Jeong Sook Ha*[,†,‡]

[†]KU-KIST Graduate School of Converging Science and Technology and [‡]Department of Chemical and Biological Engineering, Korea University, 145 Anam-ro, Seongbuk-gu, Seoul 02841, Republic of Korea

[§]School of Civil, Environmental and Architectural Engineering, Korea University, Seoul 136-713, Republic of Korea

[⊥]KU-KIST Green School, Graduate School of Energy and Environment, Korea University, Seoul 136-701, Republic of Korea

Supporting Information

ABSTRACT: A highly-durable, highly-flexible transparent electrode (FTE) is developed by applying a composite made of a thin metal grid and a doped conducting polymer onto a colorless polyimide-coated NOA63 substrate. The proposed FTE exhibits a transparency of 90.7% at 550 nm including the substrate and a sheet resistance of 30.3 Ω/sq and can withstand both moderately high-temperature annealing (~180 °C) and acidic solution (70 °C, pH 0.3) processes without performance degradation. The fabricated FTE yielded good mechanical stability under 10 000 cycles of bending deformations at a bending radius less than 1 mm without degradation of electrical conductivity. The high durability of the proposed FTE allows for the fabrication of flexible energy harvesting devices requiring harsh conditions, such as highly flexible perovskite solar cells (FPSCs) with a steady-state power conversion efficiency (PCE) of 12.7%. Notably, 93% of the original PCE is maintained after 2000 bending cycles at an extremely small bending radius of 1.5 mm. The FPSCs installed on curved surfaces of commercial devices drive them under various environments. The applicability of the proposed FTE is further confirmed via the fabrication of a flexible perovskite light-emitting diode. The proposed FTE demonstrates great potential for applications in the field of flexible optoelectronic devices.

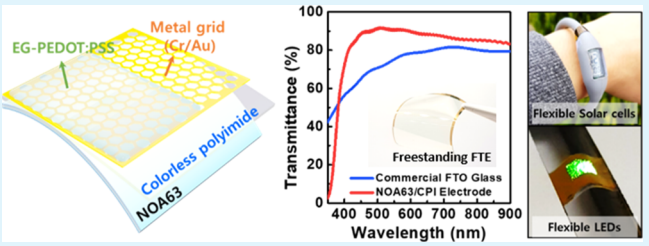

KEYWORDS: *transparent electrode, highly flexible, metal grid, conducting polymer, perovskite solar cell, light-emitting diode*

1. INTRODUCTION

In line with the increasing demand and necessity for flexible devices, relative research has been actively conducted.[1−3] Flexible devices enable a variety of applications that are impossible with conventional devices. Various materials, structures, and devices have been proposed and studied, but there are still many problems that need to be solved. Flexible optical devices are also one of the most challenging fields[4−6] owing to the difficulty in developing flexible transparent electrodes (FTEs) that simultaneously satisfy transparency, conductivity, and durability requirements. One of the most studied optoelectronic devices in recent years is perovskite solar cells. Organic−inorganic perovskite-based solar cells are emerging as next-generation flexible photonic devices owing to their inherent high optical efficiency and fair flexibility.[6,7] In addition to studying perovskite materials themselves, various studies have also been actively conducted to maximize the flexibility of transparent electrodes by introducing new materials or optimizing their structures.[6−10]

Indium-doped tin oxide (ITO, In:SnO_2) is one of the most widely used flexible transparent conductors with good performance. However, its low durability limits the range of flexible device fabrication processes and applications that can use it.[8,11,12] To overcome these limitations, various materials and structures have been proposed, such as ultrathin metal films (UTMFs),[12] carbon-based materials,[9,13,14] conducting polymers,[7,15,16] conductive meshes,[8,17−19] metal nanowires,[20] and their composites.[8,15,21] However, it is still difficult to achieve high flexibility and device processability while maintaining performance. UTMFs and metal nanowires can achieve low sheet resistance and high transparency and flexibility; however, they suffer from physical and chemical stability issues owing to the reactivity of materials such as Ag and Cu without a stable morphology.[22,23] Although graphene and carbon nanotubes have excellent mechanical durability, it is difficult to obtain a low sheet resistance when using them without sacrificing transparency because of a trade-off between transmittance and electrical conductivity.[13,14] Studies on using

Received: June 19, 2018
Accepted: August 16, 2018
Published: August 16, 2018

DOI: 10.1021/acsami.8b10190
ACS Appl. Mater. Interfaces XXXX, XXX, XXX−XXX

an intrinsically conducting polymer, namely, poly(3,4-ethylenedioxythiophene) polystyrene sulfonate (PEDOT:PSS), have also been actively conducted.[7,15,16,24−26] PEDOT:PSS is a water-dispersible polymer that can easily form a conductive thin film via spin-coating. Its excellent inherent mechanical stability also allows for repetitive bending at very small bending radii. However, despite various attempts to improve its conductivity,[15,24,27,28] it is difficult to obtain the low sheet resistance (<50 Ω/sq) required for optoelectronic device applications without increasing its thickness.[10] PEDOT:PSS is also unsuitable for high-temperature processes over 120 °C because the conductivity can be reduced due to oxidation.[29] To address these disadvantages, studies using PEDOT:PSS along with other flexible conductors are underway to develop electrodes with better conductivity and durability.[8,15] Although many conductors possess a fair flexibility, achieving high flexibility is often influenced by a variety of other factors, such as the type of applied strain,[18] the thickness of the conductor,[30,31] and the type of the substrate used.[7,16,32] Thus, achieving high flexibility (bending radius < 2 mm) is quite challenging.[7,9,12,15,21,33]

Transparent flexible substrates have major constraints that limit the flexibility and processability of flexible electrodes. Although polyethylene terephthalate (PET) and polyethylene naphthalate (PEN) are widely used, their durability hinders the development of highly flexible transparent electrodes and device fabrication processes at temperatures above the glass-transition temperatures (T_g).[3,32,34] In our preliminary investigation, Norland Optical Adhesive 63 (NOA63, Norland Products, Inc.) and colorless polyimide (CPI) were noted for their high durability, transparency, and processability.[3,7,35] It is easy to control the thicknesses of both of these polymers via spin-coating, and both are fairly durable, enabling moderately-high-temperature fabrication processes.[3,36] In particular, owing to its shape memory characteristics, NOA63 is more suitable for high-temperature processes and mechanical deformation than PET and PEN when deformed at $T > T_g$ and at a low bending radius (r < 1.2 mm).[7] However, in the case of solution processes, NOA63 becomes inadequate because its properties are plasticized by water.[35]

In this study, we demonstrated a FTE with high performance, particularly focusing on the device fabrication processability based on improved durability. Our electrodes showed excellent thermal and acidic solution processability while maintaining the performance that can be applied to actual devices via introducing a complex of nanometer-thick metal grids (Cr/Au) and ethylene glycol (EG)-doped PEDOT:PSS on a CPI-coated NOA63 substrate. Studies in this respect have not been addressed in previously reported works of similar electrode structures as shown in Table S1. The developed FTE exhibited good conductivity (<30 Ω/sq) and transparency (T_{550nm} > 90%) in addition to high mechanical stability under 10 000 bending cycles at a bending radius of 0.7 mm. Furthermore, its high stability under processes at high-temperature and acidic conditions enabled the facile growth of the metal oxides required for fabricating highly flexible perovskite solar cells (FPSCs). The fabricated FPSCs exhibited only a very small reduction in performance even after 2000 repetitive bending cycles at a very small bending radius of 1.5 mm. Finally, we managed to fabricate flexible perovskite light-emitting diodes (LEDs) using our FTEs, which suggests that they have great potential for application in various flexible optoelectronic devices.

2. EXPERIMENTAL PROCEDURES

2.1. Fabrication of a Flexible Transparent Substrate (NOA63/CPI). Before substrate fabrication, a glass slide (Matsunami micro slide glass S9213) was rinsed in sequence with detergent, distilled water, acetone, and 2-propanol. As a detachment-promoting layer for NOA63/CPI, polymethyl methacrylate (PMMA, MicroChem 495 PMMA A2) was spin-coated on the glass slide at 4000 rpm for 30 s and then annealed at 180 °C for 2 min. After that NOA63 was spin-coated on PMMA at 4000 rpm for 30 s as the main supporting substrate and cured using a 365 nm UV lamp for 40 min. A UV/ozone treatment was then carried out for 2 min. As a substance that can reinforce NOA63, CPI (Dongbaek Finechem DFCPI-301) was spin-coated on NOA63 at 4000 rpm for 50 s and sequentially annealed at 100 °C for 10 min, at 160 °C for 20 min, and at 180 °C for 20 min.

2.2. Formation of Flexible Transparent Conductors (Metal Grid + EG-PEDOT:PSS). A total of 3 nm of chromium (Cr) was deposited on the NOA63/CPI substrate as an adhesion layer for Au. Then, 60 nm of Au was deposited on the Cr layer. To form a metal grid with a honeycomb structure, photolithography and etching methods were used. A negative photoresist (MicroChem, AZ5214) was spin-coated on the Au layer at 4000 rpm for 30 s and annealed on a hot plate at 110 °C for 1 min. After that the photoresist was patterned using a photomask and a mask aligner (MIDAS system, MDA-400M) via selective exposure to UV light for 6 s. A developer (Merck, AZ 300 MIF Developer) was used to remove the UV-exposed photoresist; the electrode was then rinsed with deionized (DI) water. The exposed Au was removed by immersing the electrode in an Au etchant (Transene, Gold Etch-Type TFA) for 20 s and then rinsing with DI water. Afterward, it was exposed to UV light (325 nm) for 1 min, and the remaining photoresist was removed with flowing 2-propanol. Then, the exposed Cr was removed by immersing the electrode in a Cr etchant (Aldrich, Chromium Etchant) for 1−2 s and rinsing it with DI water. The grid-patterned electrode was treated overnight with a 3-(aminopropyl)triethoxysilane aqueous solution to enhance the adhesion between EG-PEDOT:PSS and the NOA63/CPI substrate.[37] As the transparent conductor of the window part of the device, PEDOT:PSS (Clevios, PH1000) doped with 5 wt % EG was spin-coated on the grid electrode at 2000 rpm for 1 min and then cured at 120 °C for 20 min.

2.3. Modification of the FTE for Its Cathodic Application in Flexible Perovskite Solar Cells. First, EG-PEDOT:PSS was patterned to form the solar cell electrode via a O_2 reactive-ion etching (RIE) process (chamber pressure: 0.13 Torr, O_2 flow: 20 sccm, power: 100 W, time: 1 min). Then, 6 nm of titanium was deposited for energy band alignment. After a UV/O_3 treatment that lasted 15 min, a 0.1 M aqueous solution of $SnCl_4$ was spin-coated at 5000 rpm for 10 s and annealed at 180 °C for 1 h to form the SnO_2 layer. Then, a rutile TiO_2 layer was grown by immersing the UV/O_3-treated (10 min) sample in an aqueous solution of $TiCl_4$ (70 °C, 200 mM) for 30 min. After washing the $TiCl_4$-treated samples with DI water and ethanol, they were annealed at 100 °C on a hotplate for 1 h.

2.4. Fabrication of Flexible Perovskite Solar Cells. All precursor materials were prepared as described in a previous report.[38] A 1.4 M $(FAPbI_3)_{0.95}(MAPbBr_3)_{0.05}$ solution was prepared by dissolving $NH_2CH{=}NH_2I$ (FAI) and CH_3NH_3Br (MABr) with PbI_2 and $PbBr_2$ in *N*,*N*-dimethylformamide (DMF) and dimethylsulfoxide (8:1 v/v) by stirring at 60 °C for 1 h. Then, the solution was coated onto the FTE/Ti/SnO_2/TiO_2 sample, which was fabricated according to the abovementioned method, in two consecutive spin-coating steps at 1000 and 5000 rpm for 5 and 10 s, respectively. During the second spin-coating step, 1 mL of ethyl ether was poured onto the substrate after 5 s. Then, the substrate was thermally treated at 150 °C for 10 min. A compact $(FAPbI_3)_{0.95}(MAPbBr_3)_{0.05}$ film with a thickness of 550 nm was obtained. A spiro-OMeTAD/chlorobenzene (100 mg/1.1 mL) solution with additives of 23 μL of Li-bis(trifluoromethanesulfonyl)imide/acetonitrile (540 mg/1 mL), 39 μL of 4-*tert*-butylpyridine, and 10 of μL tris(2-(1*H*-pyrazol-1-yl)-4-*tert*-butylpyridine)-cobalt(III)tris(bis-(trifluoromethylsulfonyl)imide):(FK209)/acetonitrile (376 mg/1

DOI: 10.1021/acsami.8b10190
ACS Appl. Mater. Interfaces XXXX, XXX, XXX−XXX

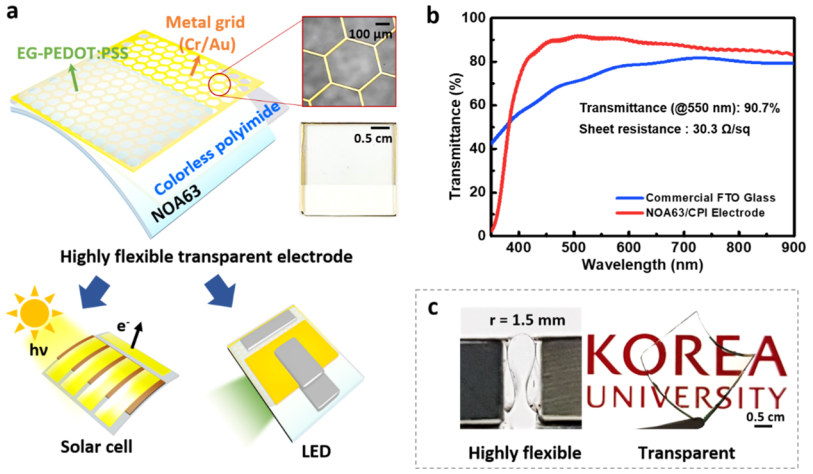

Figure 1. (a) Schematic illustration of the fabricated FTE for perovskite optoelectronic devices (solar cells and LEDs). (b) Transmittance spectrum of the FTE compared with that of commercial fluorine-doped tin oxide (FTO) glass. (c) Optical images of the fabricated FTE.

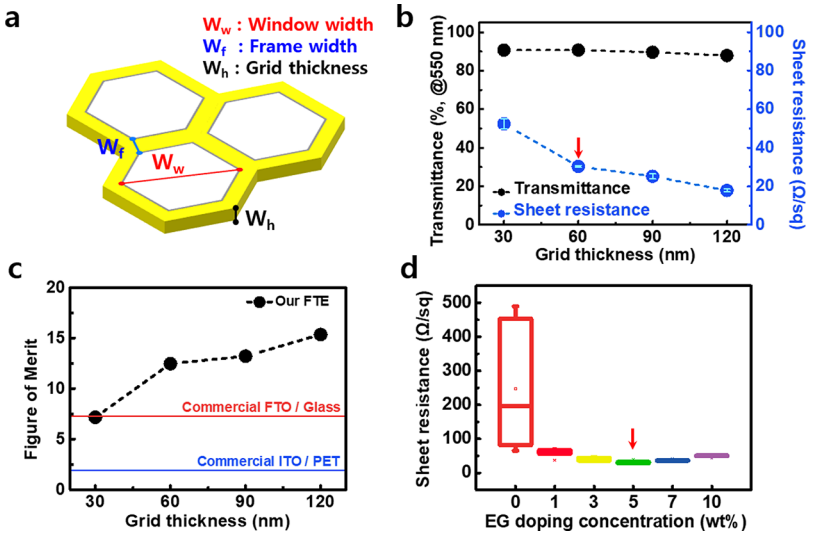

Figure 2. (a) Schematic illustration of the metal grid with a honeycomb structure. W_w, W_f, and W_h are defined. (b) Transparency (transmittance) and sheet resistance of the developed FTE according to grid thickness. (c) Figure of merit according to grid thickness. (d) Changes in sheet resistance according to the EG doping concentration. Here, the red arrows in (b,d) indicate the selected conditions used in subsequent application experiments.

mL) was spin-coated on the FTE/Ti/SnO_2/TiO_2/$(FAPbI_3)_{0.95}(MAPbBr_3)_{0.05}$ perovskite layer at 2000 rpm for 30 s. Finally, an Au counter electrode was deposited via thermal evaporation while its active area was fixed at 0.16 cm^2.

2.5. Fabrication of a Flexible Perovskite LED. Before LED fabrication, the FTE was patterned via O_2 RIE. The LED fabrication process was conducted as described before.[39] A polyethylene oxide (PEO) solution (10 mg/mL) was prepared by dissolving PEO (M_w 8 000 000, Aldrich) in DMF (Aldrich, anhydrous). A $MAPbBr_3$ ($CH_3NH_2PbBr_3$) precursor solution was prepared by dissolving 343 mg of lead(II) bromide and 157 mg of methylammonium bromide in 1 mL of DMF. Both solutions were stirred on an 80 °C hotplate for 20 min. PEO/$MAPbBr_3$ reagents were prepared by mixing the two prepared solutions at a mass ratio of 1.5:1 (PEO solution/$MAPbBr_3$ solution). Another PEO solution (1.3 mg/mL) was prepared by diluting 0.5 mL of the previously prepared PEO solution (10 mg/mL) with 3.5 mL of DMF. All solutions were placed on an 80 °C hotplate before coating. First, the PEO solution (1.3 mg/mL) was spin-coated onto the patterned FTE at 6000 rpm for 40 s and annealed at 80 °C for 5 min. Then, the PEO/$MAPbBr_3$ solution was spin-coated at 1000 rpm for 6 min until the film color turned orange. After that it was annealed on an 80 °C hotplate for 20 min. Finally, the top electrodes were formed by spray-coating square-patterned liquid metal Galinstan (GaInSn) using a shadow mask.

2.6. Characterization. The surface morphology of the fabricated FTE was investigated using a scanning electron microscope (Hitachi S-4800). The sheet resistance of the fabricated electrode was measured using a four-point probe (Desk 205, MS Tech) with a source measurement unit (Keithley 2400 SourceMeter). The current density−voltage (J−V) characteristics of all of the fabricated devices were measured using an AM 1.5G solar simulator and an electrochemical analyzer (Ivium Technologies, Compact Stat.).

3. RESULTS AND DISCUSSION

3.1. Schematic Illustration of the Fabricated FTEs. Figure 1a shows the developed FTE, which is composed of a durable, highly flexible transparent substrate (NOA63/CPI) and highly conductive transparent conductors (EG-doped PEDOT:PSS with Cr/Au metal grids). Therefore, it can be used for fabricating recently spotlighted perovskite solar cells and LEDs. The fabricated electrode is highly transparent, flexible, and conductive, as shown in Figure 1b,c. Although the NOA63/CPI substrate provides high flexibility and high

DOI: 10.1021/acsami.8b10190
ACS Appl. Mater. Interfaces XXXX, XXX, XXX−XXX

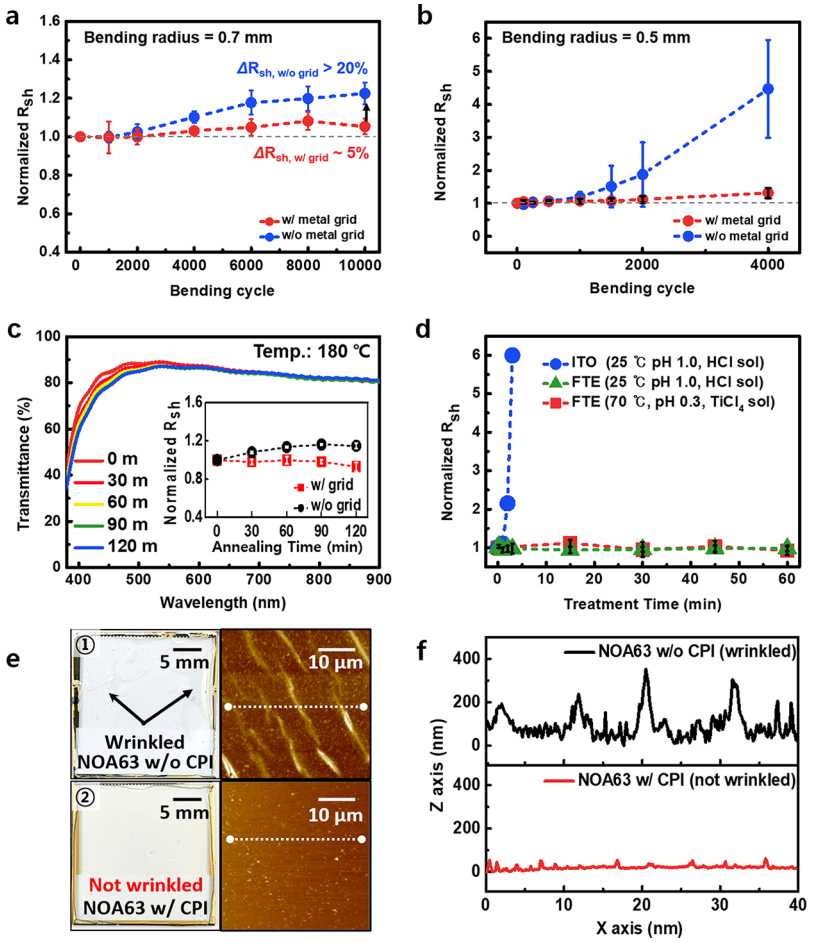

Figure 3. Changes in the sheet resistance of the FTE with or without a metal grid, along with the results of repetitive bending tests at bending radii of (a) 0.7 and (b) 0.5 mm, respectively. (c) Changes in the transmittance of our FTE after annealing at 180 °C for up to 2 h. The inset shows sheet resistance vs annealing time with and without using the grid. (d) Changes in the sheet resistance of the FTE under different chemical treatments. (e) Surface morphology after a $TiCl_4$ chemical bath deposition (CBD) process depending on the existence of coated CPI, measured using an optical microscope (left) and an atomic force microscope (right). (f) Atomic force microscopy line profiles of the surfaces without (top) and with (bottom) CPI, respectively.

durability, both the design of the metal grid and the doping concentration of EG were optimized to achieve high conductivity and transparency for flexible optoelectronic device applications. A FTE with high performance (R_{sh} < 30 Ω/sq, T_{550nm} > 90%) and durability (processable temperature: ~180 °C, flexibility: 10 000 bending cycles at bending radius <1 mm, acid resistance: 70 °C, pH 0.3) was realized through these efforts. A facile detaching process was also developed to make the fabricated electrodes or devices freestanding by exploiting the weak adhesion between PMMA and the NOA63 substrate. This allows the fabricated device and electrode to be smoothly peeled off from the glass substrate at any desired stage without using a chemical lift-off process that could damage the device (Figure 1c). In addition, without PMMA, the fabricated device would be damaged during the dry detachment process because of the strong adhesion between NOA63 and the glass substrate. Furthermore, owing to modifications of the process made possible by the heat and acid resistance of our FTE, some useful metal oxides (TiO_2, SnO_2) could be directly grown on the FTE, as described in section 3.4. Various applications, including FPSCs, LEDs, and driving real-life devices, are shown below to demonstrate that the FTE fabricated in this study can be used in practical optoelectronic devices.

3.2. Performance of the Fabricated FTE. To verify that the performance of the FTEs depends on the materials and structures used, their sheet resistance (R_{sh}) and transparency were measured under various conditions.

Figure 2a shows the honeycomb structure of our metal grid. In the figure, the window width (W_w), the frame width (W_f), and the grid thickness (W_h) are defined. As shown in Figure S1, when the frame width of the metal grids was reduced to less than 30 μm while keeping the opening ratio (OR) at 95.2%, the measured conductivity and its uniformity were improved in a single electrode. As metal grids become finer, the carrier paths composed of EG-PEDOT:PSS for reaching them become shorter. Thus, this leads to an increase in the measured conductivity. In fact, as the window width (W_w) becomes wider, the nonuniformity of the measured R_{sh} increases because the distance between the four-probe measuring unit and the metal grids depends on the measurement position. To verify that the electrode performance varies with the thickness of metal grid, R_{sh} and the transparency of the electrodes were measured as the thickness of Au was varied while the grid design remained the same. In these experiments, the thickness of Cr was fixed at 3 nm, whereas that of gold was changed. As expected, as the grid thickness (W_h) increased and the sheet resistance of the FTE

DOI: 10.1021/acsami.8b10190
ACS Appl. Mater. Interfaces XXXX, XXX, XXX−XXX

decreased, whereas the transparency remained almost unchanged, as shown in Figure 2b, because the thickness of the grid does not affect the OR of the metal grids. To evaluate the performance of the FTEs, the figure of merit was calculated using the following equation[17,21]

$$\text{Figure of merit} = \frac{T^{10}}{R_{sh}} \quad (1)$$

where R_{sh} is the sheet resistance of the FTE and T is the transmittance value of the FTE at 550 nm. Because the overall transparency of the FTE is important in actual device applications, the transparency of the substrate was also included. Figure 2c shows that the developed FTE has a higher figure of merit than commercial FTO glass and ITO/PET electrodes. A 3/60 nm thick Cr/Au grid was adopted because a sufficiently low sheet resistance (~30 Ω/sq) and a high figure of merit (>12.5) could be obtained without deteriorating the overall roughness and the thickness of the FTE. Because of the wide width of the grid window, pristine PEDOT:PSS (PH1000, 0.9 S cm^{-1})[8] is not adequate as the conductor of the window portion as shown in Figure 2d. To solve this problem, EG was added to pristine PEDOT:PSS, which increased the conductivity by about 3 orders of magnitude by rearranging the molecules in the PEDOT:PSS film.[27,28] For concentrations between 1 and 10 wt %, the deviation of measured R_{sh} via repeated four-probe measurements was small, and the lowest R_{sh} was obtained at a doping concentration of approximately 5 wt %. On the basis of these observations, it can be confirmed that the PEDOT:PSS plays an important role as a transparent conductor of the window portion that collects electrons and transports them to nearby metal grids.

3.3. High Durability of the Fabricated FTE. *3.3.1. High Flexibility of the Fabricated FTE.* The major advantage of the fabricated electrode is its super-flexibility. To verify the mechanical durability of the fabricated FTE, bending tests were carried out at various bending radii ranging from 5 to 0.5 mm, as shown in Figures 3a,b and S2. As can be seen in Figure 3a, there was no noticeable change in sheet resistance even after 10 000 cycles of repeated bending at an extremely small bending radius of 0.7 mm when using the metal grid. Using EG-PEDOT:PSS with a grid ($\Delta R_{sh,w/grid} \approx 5\%$) does outperform using it without a grid ($\Delta R_{sh,w/o\ grid} > 20\%$) for its robust mechanical properties. This phenomenon can be attributed to the honeycomb structure of the metal grids, which prevents the propagation of cracking or peeling of the grid and PEDOT:PSS.[19,40] However, at r = 0.5 mm, the sheet resistance increased rapidly after approximately 2000 bending cycles because of the mechanical damages formed on the flexible electrode, as shown in Figures 3b and S2d. We believe that this could be improved by optimizing the thickness of the substrate in the future studies. These results show that the mechanical strength of the fabricated FTE is much higher than that of ITO/PET, which is large-domain damaged even after 100 bending cycles at a bending radius of 5 mm, as shown in Figure S2c.

It is worth re-emphasizing that achieving such high flexibility is highly challenging owing to the influence of many factors. In previous studies, it was reported that metal grid or conducting polymer-based transparent electrodes were often damaged by repetitive bending at bending radii of less than 3 mm.[16,18] This is mainly due to crack formation in the thick metal grids or the delamination of the conducting polymers. We speculate that the high flexibility of the developed FTE can be attributed to the thin (~60 nm) metal grids used with better fatigue resistance than thicker (>1 μm) ones.[30,31] By using EG-PEDOT:PSS, which has improved conductivity, even a very thin grid could ensure a sufficiently low sheet resistance for device fabrication.

3.3.2. Thermal Stability of the Fabricated FTE. Another notable advantage of the developed FTE is that it has excellent durability at quite high temperatures. As shown in Figures 3c and S3, the transparency and R_{sh} of the FTEs were measured for annealing temperatures between 140 and 200 °C at intervals of 30 min for 2 h. Their performance was maintained even after annealing at 180 °C for 2 h. At 200 °C, however, their transparency decreased with annealing time owing to the denaturation of the NOA63 substrate, as shown in Figure S3b. One noticeable phenomenon was that the use of EG-PEDOT:PSS and metal grids at the same time prevented the rapid degradation of the performance of the electrodes during long annealing processes (see the insets of Figures 3c and S3). Generally, when a PEDOT:PSS-based transparent electrode is heated to temperatures above 120 °C, its conductivity is lowered owing to oxidation.[29] However, in the proposed structure, even if PEDOT:PSS is slightly oxidized, it has almost no influence on R_{sh}. We think that EG-PEDOT:PSS, with its greatly improved conductivity, can facilely transfer carriers to the metal grid even after high-temperature annealing.

The high thermal stability of our FTEs could be used to successfully fabricate highly FPSCs, for which the growth of SnO_2 at 180 °C should be done without degradation of the FTE, as explained in section 3.4.

3.3.3. Chemical Stability and Solution Processability of the Fabricated FTEs. To investigate the chemical stability and solution processability of the fabricated FTEs, their performance was measured after treating them with an acid solution at room temperature (25 °C) and at a higher temperature (70 °C) for a certain time. As shown in Figure 3d, PET/ITO electrodes lost their conductivity within 4 min in a 25 °C, pH 1.0 hydrochloric acid (HCl) aqueous solution because HCl solutions rapidly etch ITO.[11] However, the FTEs fabricated in this study retained their performance for 1 h under the same conditions and even in harsher conditions (70 °C, pH 0.3, 200 mM $TiCl_4$ aqueous solution).

Because NOA63 can be plasticized by water,[35] deformation (wrinkles) occurs when a solution process is carried out for a long period of time with a NOA63-only substrate, as can be seen in Figure 3e(1). These wrinkles cause the quality of the film to deteriorate during further device fabrication steps because wrinkles of several hundred nanometers in height hinder uniform film formation during the spin-coating processes. Thanks to the CPI coating on the NOA63 surfaces, the former of which has a high glass-transition temperature of approximately 300 °C,[41] the deformations mentioned above were retrained effectively [Figure 3e(2)]. Because of the materials used in our electrodes, a simple and effective solution processability of FTEs was obtained here. Owing to their high stability under harsh conditions, CBD of rutile TiO_2 films could be conducted successfully, as shown in section 3.4, which is suitable to the fabrication of high-performance perovskite solar cells.

3.4. Modification of the Fabricated FTE for Perovskite Solar Cell Applications. To apply our FTE for the fabrication of perovskite solar cells, we modified the electrodes

DOI: 10.1021/acsami.8b10190
ACS Appl. Mater. Interfaces XXXX, XXX, XXX−XXX

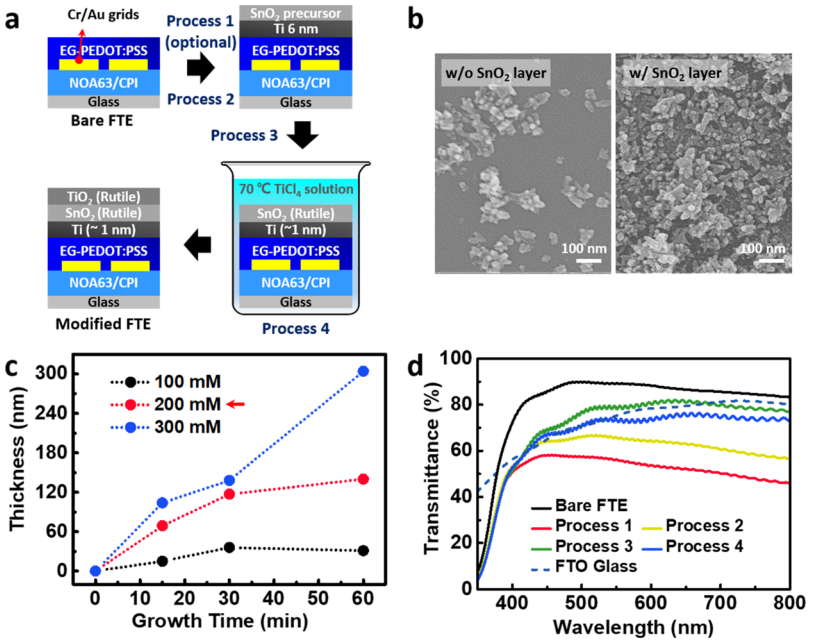

Figure 4. (a) Schematic illustration of the electrode modification process. (b) SEM images of TiO_2 grown on a Si substrate under $TiCl_4$ treatment conditions and the presence of a SnO_2 layer. (c) Thickness of the grown TiO_2 for different $TiCl_4$ solution concentrations and growth times. The red arrow indicates the conditions selected for the fabrication of optoelectronic devices in this work. (d) Changes in electrode transparency over the different process steps described in (a).

on which the metal oxide could be grown, as shown in Figure 4a. Because the growth of metal oxide requires processes under harsh conditions, such as high-temperature annealing at 180 °C for SnO_2 (process 3) and acidic (pH 0.3) and solution process at 70 °C for CBD of TiO_2 (process 4), the high durability of our fabricated FTE is energetically favored for such harsh processes, in contrast to the conventionally used ITO/PET electrodes. CBD (process 4) using $TiCl_4$ is a simple, low-temperature (~70 °C) solution process for the direct growth of rutile TiO_2 thin films on a substrate.[42,43] However, owing to the following two limitations, this process has been mainly performed on rigid FTO (F:SnO_2) glasses rather than on the flexible ITO/PET electrodes. First, approximately an hour in a strong acid solution (pH 0.3) at 70 °C is required, which may etch out ITO.[11] Second, this process was tested only on a FTO substrate because rutile TiO_2 grows compactly only when the substrate crystallinity is matched.[42−44] In this study, we found that rutile TiO_2 can be grown compactly on a nanocrystalline SnO_2 layer,[45,46] providing surface properties similar to F:SnO_2. Thus, rutile TiO_2 CBD can be promoted even on substrates other than FTO. Our scanning electron microscopy (SEM) images, along with our X-ray diffraction and X-ray photoelectron spectroscopy analyses, confirmed that TiO_2 growth was promoted when the SnO_2 layer was present, as shown in Figures 4b, S6, and S8. By adjusting the concentration of the $TiCl_4$ solution and growth time, the thickness and morphology of TiO_2 grown via CBD can be easily controlled, as shown in Figures 4c and S6. However, in $TiCl_4$ solutions with high concentrations (above 300 mM), the TiO_2 film becomes very thick, causing cracking and peeling and making it unsuitable for device fabrication (Figure S7). On the basis of previous $TiCl_4$ CBD studies on FTO electrodes, we selected the optimal concentration of 200 mM. $TiCl_4$ concentration determines the size of the grown rutile TiO_2 crystals.[43] It is worth mentioning that there have been several reports on treating SnO_2 with $TiCl_4$ to improve the efficiency of electron transport. To the best of our knowledge, this work is the first to report the use of SnO_2 to enable TiO_2 CBD on flexible substrates other than FTO.[47,48] These results suggest that such techniques can be used for various types of flexible transparent applications based on metal oxides.

At this stage, 6 nm thick titanium is deposited on the FTE (process 1), especially for n−i−p-structured solar cell applications, as shown in Figure 4a. In general, PEDOT:PSS-based electrodes are used as p-type electrodes because they have a high work function (~5.0 eV).[49] In this study, however, the work function of the FTEs was lowered by depositing titanium with a relatively low work function.[50] Then, the growth of electron-transporting SnO_2 and TiO_2 resulted in the fabrication of n-type FTEs through the process shown in Figure 4a. Even though the deposition of a 6 nm thick Ti film causes significant degradation in the transparency of the electrode in the early stages of the process, as shown in Figure 4d, it was necessary to use that thickness considering the loss of some Ti in subsequent SnO_2 formation processes (process 2 and process 3 in Figure 4a). In the optimization process, the initial thickness was adjusted to 6 nm so that finally 1−2 nm thick titanium remained (Figure S5). After the growth of SnO_2 (process 2 and process 3 in Figure 4a,d) was completed, the transparency of the electrode was increased in two steps. The first step (process 2) is a UV/O_3 treatment before the spin-coating of a $SnCl_4$ aqueous solution. This UV/O_3 treatment, which lasts 5−15 min, causes the oxidation of the Ti film,[51,52] turning the opaque Ti into transparent TiO_2.[53] The second step (process 3) is a sintering process at 180 °C for 1 h after coating with a $SnCl_4$ solution. The formation of the SnO_2 layer through the sintering of $SnCl_4$ occurs as follows[46]

DOI: 10.1021/acsami.8b10190
ACS Appl. Mater. Interfaces XXXX, XXX, XXX−XXX

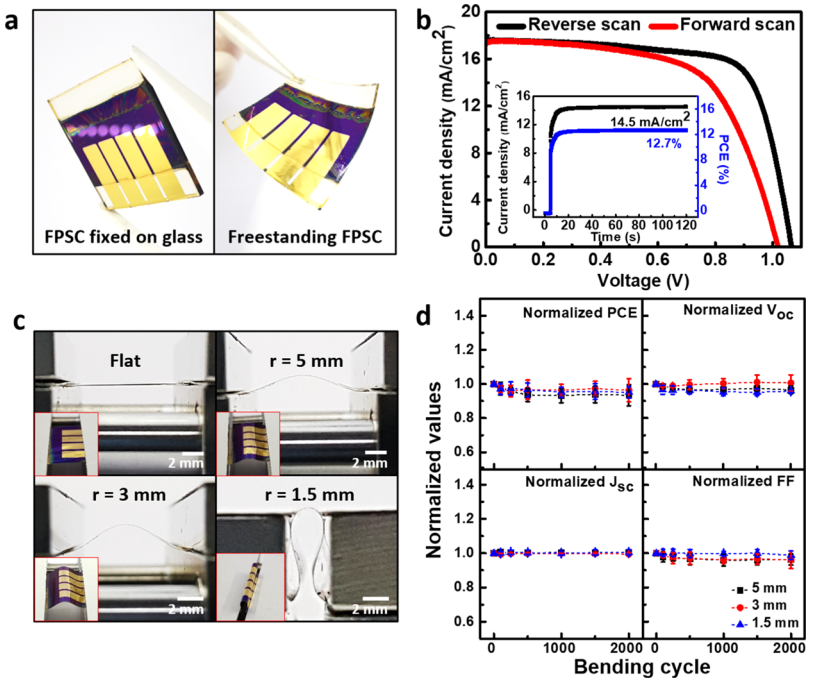

Figure 5. (a) Optical images of the fabricated FPSC (left) fixed on a glass substrate and (right) freestanding. (b) Current density vs voltage curve of the fabricated FPSC. The inset shows its steady-state current and power conversion efficiency (PCE). (c) Optical images of the bent FPSCs at various bending radii. (d) Changes in solar cell performance vs bending cycle for different bending radii.

$$SnCl_4 + 4H_2O \rightarrow Sn(OH)_4 + 4HCl$$
$$Sn(OH)_4 \rightarrow H_2SnO_3 + H_2O$$
$$H_2SnO_3 + 2HCl \rightarrow SnOCl_2 + 2H_2O \quad (2)$$

We speculate that HCl and Sn^{2+} ions generated in this process might promote the oxidation of Ti. It is known that hydrochloric acid solutions also etch Ti, but their etching rate is too slow to account for the observed phenomenon.[54] Therefore, it can be deduced that the presence of Sn^{2+} ions accelerates the oxidation of Ti because the standard reduction potential of Ti ($E^{\circ}_{Ti/Ti^{2+}} = -1.63$ V) is smaller than that of Sn ($E^{\circ}_{Sn/Sn^{2+}} = -0.13$ V).[55] As a result, the FTEs fabricated in this study could maintain a transparency corresponding to that of FTO glass even after the modification process, as shown in Figure 4d.

3.5. Application. *3.5.1. Highly Flexible Perovskite Solar Cells Based on the Fabricated FTEs.* Organic−inorganic perovskite-based solar cells are emerging as next-generation flexible photonic devices owing to their high optical efficiency and their fair flexibility.[3,7,9] Here, highly FPSCs were successfully fabricated using the developed FTEs with Ti/SnO_2/TiO_2 multilayers, as shown in Figures 5a and S4. The fabrication procedure is described in the section titled Experimental Procedures. We used a mixed perovskite halide material made of formamidinium lead iodide ($FAPbI_3$) and methylammonium lead bromide ($MAPbBr_3$), which have shown superior photovoltaic performance with high phase stability.[38] The FPSCs had an n−i−p device architecture, namely, NOA63/CPI/Cr:Au mesh_EG-PEDOT:PSS/Ti/SnO_2/TiO_2/$(FAPbI_3)_{0.95}(MAPbBr_3)_{0.05}$/spiro-MeOTAD/Au, based on the suitable band energy alignments between each of the layers, as shown in Figure S4.

The current density−voltage (J−V) curves and the steady-state photocurrent at maximum power for the FPSCs were measured under AM 1.5G illumination conditions at 25 °C and are presented in Figure 5b. The fabricated FPSCs exhibited hysteresis in the J−V curves with reverse and forward sweeps. The J_{sc}, V_{oc}, and FF values obtained from the J−V curves in the reverse sweep mode were 17.6 mA·cm^{-2}, 1.07 V, and 0.72, respectively, yielding a PCE of 13.6%. The corresponding values obtained from the J−V curve in the forward scan mode were 17.3 mA·cm^{-2}, 1.02 V, and 0.62, respectively, yielding a lower overall efficiency of 11.4%. The hysteresis could be attributed to the planar device architecture without a mesoporous TiO_2 layer, which is not feasible for the fabricated FTEs owing to the high annealing temperature of 500 °C used.[56] Therefore, a stabilized PCE was estimated to find the real power output of the device by measuring the steady-state photocurrent with the applied voltage at the maximum power point in the inset of Figure 5b. A stable steady-state photocurrent density of 14.5 mA·cm^2 was measured at V_{mpp} of 0.88 V under 1 sun standard conditions, yielding a stabilized PCE of 12.7% for the FPSCs.

To confirm the mechanical stability of the fabricated solar cells, bending tests were performed for 2000 cycles at bending radii ranging from 5 to 1.5 mm, as shown in Figure 5c,d. The FPSC fabricated and used in this experiment maintained 93% of its original PCE, 96% of its original V_{oc}, 98% of its original FF, and there was almost no change in J_{sc} even after 2000 cycles of bending at a very small bending radius of 1.5 mm. From these results, we confirmed that the fabricated FTE can maintain its performance and mechanical durability even after the complete fabrication processes of the perovskite solar cell. These findings are rare, as very few studies have reported highly FPSCs that can withstand repetitive bending at an extremely small bending radius of 1.5 mm.[7,57]

3.5.2. Charging and Driving of Real-Life Devices Using the Fabricated FPSCs. Next, we demonstrate that our FPSCs can drive commercial devices. After attaching a FPSC onto the

DOI: 10.1021/acsami.8b10190
ACS Appl. Mater. Interfaces XXXX, XXX, XXX−XXX

curved surface of a liquid crystal display (LCD) wristwatch, it was connected to the LCD without a battery. As shown in Figure 6a and Movie S1, under natural light, we observed that

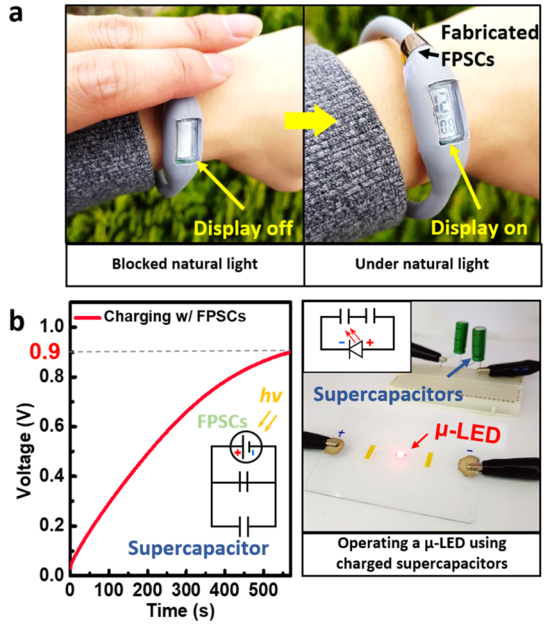

Figure 6. (a) LCD watch driven by our fabricated FPSC attached onto its curved band in an outdoor/natural light environment. (left) Display turned off by blocking and (right) display turned on by illuminating the FPSC with sunlight. (b) (left) Charging of supercapacitors using FPSCs and (right) driving a red micro-LED (μ-LED) with supercapacitors charged with FPSCs.

the LCD watch was driven stably by the FPSC. When the light was blocked, the LCD watch stopped working, as expected. Additional experiments were conducted to charge commercial energy storage devices with the fabricated FPSCs, as shown in Figure 6b. Two 3 F supercapacitors were connected in parallel and charged to 0.9 V. Then, a red μ-LED was driven by the charged supercapacitors. The LED maintained its maximum brightness for approximately 7 min, as shown in Figure 6b.

3.5.3. Flexible Perovskite LED Based on the Fabricated FTE. Finally, we demonstrate the application of our FTE to photonic devices other than solar cells. Figure 7a shows the structure of a green LED fabricated using our electrodes. A simple, flexible perovskite LED was fabricated by coating the fabricated FTE with a perovskite-based luminescent material, namely, PEO/$MAPbBr_3$, and by forming the upper electrode with a liquid metal (GaInSn) patterned into a square via spray deposition. As shown in Figure 7, we confirmed that the fabricated rectangular green LED was well lit in both flat (Figure 7b) and bent states (Figure 7c).

4. CONCLUSIONS

A high-performance highly flexible transparent electrode with high mechanical and chemical durability was developed using a NOA63/CPI substrate, a nanothick Cr/Au grid, and EG-PEDOT:PSS. The fabricated FTE could withstand high temperatures, strong acidic solution processes, and repeated bending at an extremely small bending radius of less than 1 mm. Taking advantage of the durability of our FTEs, we developed a modification process for growing compact metal oxide (SnO_2, TiO_2) layers on the FTE, which can be applied for the development of optoelectronic devices. We demonstrated the fabrication of n−i−p-structured FPSCs using our FTEs as n-type electrodes. Our fabricated FPSC maintained a stable performance even after 2000 cycles of bending deformations at a bending radius of 1.5 mm. Various commercial devices were driven using our FPSCs, in addition to the fabrication of a flexible perovskite LED using our FTE. Such demonstrations suggest that the developed electrodes guarantee stable performance in real applications under various environments. Our work gives rise to positive expectations for better processability and an extensive range of material selections for flexible perovskite optoelectronic applications.

■ ASSOCIATED CONTENT

Supporting Information

The Supporting Information is available free of charge on the ACS Publications website at DOI: 10.1021/acsami.8b10190.

Comparison of our electrode with recently reported flexible transparent ones using similar transparent conductors; transparency and sheet resistance of the developed FTE according to the frame width of the metal grid; changes in sheet resistance of the FTE and ITO/PET; changes in the transmittance of our FTE after annealing; characterization of the fabricated FPSC; changes in transparency of fabricated FTEs according to the thickness of Ti; SEM images of rutile TiO_2 grown under different growth conditions; SEM image of cracks formed during prolonged growth at a high concentration of $TiCl_4$; and characterization of TiO_2 grown via CBD (PDF)

A LCD clock driven by a FPSC under natural light (AVI)

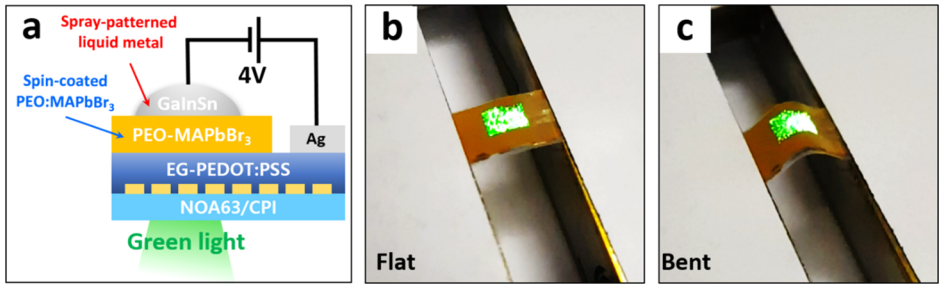

Figure 7. (a) Schematic illustration of the fabricated perovskite LED using the fabricated FTE. Optical images of a fabricated flexible LED emitting green light in (b) flat and (c) bent states (r = 3 mm).

DOI: 10.1021/acsami.8b10190
ACS Appl. Mater. Interfaces XXXX, XXX, XXX−XXX

AUTHOR INFORMATION

Corresponding Authors

*E-mail: junhnoh@korea.ac.kr. Phone: +82-2-3290-4866 (J.H.N.).
*E-mail: jeongsha@korea.ac.kr. Phone: +82-2-3290-3303 (J.S.H.).

ORCID

Jeong Sook Ha: 0000-0003-1358-3295

Author Contributions

‖S.W.J. and Y.H.L. contributed equally to this work.

Notes

The authors declare no competing financial interest.

ACKNOWLEDGMENTS

This work was supported by the National Research Foundation of Korea (NRF) grant funded by the Korean Government (MSIP) (no. NRF-2016R1A2A1A05004935). The authors also thank the KU-KIST Graduate School Program of the Korea University. S.W.J. and Y.H.L. contributed equally to this work.

REFERENCES

(1) Kim, D.-H.; Ghaffari, R.; Lu, N.; Rogers, J. A. Flexible and Stretchable Electronics for Biointegrated Devices. *Annu. Rev. Biomed. Eng.* **2012**, *14*, 113−128.

(2) Harris, K. D.; Elias, A. L.; Chung, H.-J. Flexible Electronics under Strain: A Review of Mechanical Characterization and Durability Enhancement Strategies. *J. Mater. Sci.* **2016**, *51*, 2771−2805.

(3) Park, J.-I.; Heo, J. H.; Park, S.-H.; Hong, K. I.; Jeong, H. G.; Im, S. H.; Kim, H.-K. Highly flexible InSnO electrodes on thin colourless polyimide substrate for high-performance flexible CH 3 NH 3 PbI 3 perovskite solar cells. *J. Power Sources* **2017**, *341*, 340−347.

(4) Lin, H.-Y.; Sher, C.-W.; Lin, C.-H.; Tu, H.-H.; Chen, X. Y.; Lai, Y.-C.; Lin, C.-C.; Chen, H.-M.; Yu, P.; Meng, H.-F.; Chi, G.-C.; Honjo, K.; Chen, T.-M.; Kuo, H.-C. Fabrication of Flexible White Light-Emitting Diodes from Photoluminescent Polymer Materials with Excellent Color Quality. *ACS Appl. Mater. Interfaces* **2017**, *9*, 35279−35286.

(5) Luo, Q.; Ma, H.; Hao, F.; Hou, Q.; Ren, J.; Wu, L.; Yao, Z.; Zhou, Y.; Wang, N.; Jiang, K.; Lin, H.; Guo, Z. Carbon Nanotube Based Inverted Flexible Perovskite Solar Cells with All-Inorganic Charge Contacts. *Adv. Funct. Mater.* **2017**, *27*, 1703068.

(6) Li, L.; Zhang, S.; Yang, Z.; Berthold, E. E. S.; Chen, W. Recent Advances of Flexible Perovskite Solar Cells. *J. Energy Chem.* **2018**, *27*, 673−689.

(7) Park, M.; Kim, H. J.; Jeong, I.; Lee, J.; Lee, H.; Son, H. J.; Kim, D.-E.; Ko, M. J. Mechanically Recoverable and Highly Efficient Perovskite Solar Cells: Investigation of Intrinsic Flexibility of Organic-Inorganic Perovskite. *Adv. Energy Mater.* **2015**, *5*, 1501406.

(8) Li, Y.; Meng, L.; Yang, Y. M.; Xu, G.; Hong, Z.; Chen, Q.; You, J.; Li, G.; Yang, Y.; Li, Y. High-Efficiency Robust Perovskite Solar cells on Ultrathin Flexible Substrates. *Nat. Commun.* **2016**, *7*, 10214.

(9) Yoon, J.; Sung, H.; Lee, G.; Cho, W.; Ahn, N.; Jung, H. S.; Choi, M. Superflexible, High-Efficiency Perovskite Solar Cells Utilizing Graphene Electrodes: Towards Future Foldable Power Sources. *Energy Environ. Sci.* **2017**, *10*, 337−345.

(10) Sun, K.; Li, P.; Xia, Y.; Chang, J.; Ouyang, J. Transparent Conductive Oxide-Free Perovskite Solar Cells with PEDOT:PSS as Transparent Electrode. *ACS Appl. Mater. Interfaces* **2015**, *7*, 15314−15320.

(11) Bechara, R.; Petersen, J.; Gernigon, V.; Lévêque, P.; Heiser, T.; Toniazzo, V.; Ruch, D.; Michel, M. PEDOT:PSS-Free Organic Solar Cells Using Tetrasulfonic Copper Phthalocyanine as Buffer Layer. *Sol. Energy Mater. Sol. Cells* **2012**, *98*, 482−485.

(12) Kang, H.; Jung, S.; Jeong, S.; Kim, G.; Lee, K. Polymer-Metal Hybrid Transparent Electrodes for Flexible Electronics. *Nat. Commun.* **2015**, *6*, 6503.

(13) Dai, X.; Wu, J.; Qian, Z.; Wang, H.; Jian, J.; Cao, Y.; Rummeli, M. H.; Yi, Q.; Liu, H.; Zou, G. Ultra-Smooth Glassy Graphene Thin Films for Flexible Transparent Circuits. *Sci. Adv.* **2016**, *2*, e1601574.

(14) Xu, H.; Chen, L.; Hu, L.; Zhitenev, N. Contact Resistance of Flexible, Transparent Carbon Nanotube Films with Metals. *Appl. Phys. Lett.* **2010**, *97*, 143116.

(15) Lim, J.-E.; Lee, S.-M.; Kim, S.-S.; Kim, T.-W.; Koo, H.-W.; Kim, H.-K. Brush-Paintable and Highly Stretchable Ag Nanowire and PEDOT:PSS Hybrid Electrodes. *Sci. Rep.* **2017**, *7*, 14685.

(16) Cho, C.-K.; Hwang, W.-J.; Eun, K.; Choa, S.-H.; Na, S.-I.; Kim, H.-K. Mechanical Flexibility of Transparent PEDOT:PSS Electrodes Prepared by Gravure Printing for Flexible Organic Solar Cells. *Sol. Energy Mater. Sol. Cells* **2011**, *95*, 3269−3275.

(17) Kim, W.-K.; Lee, S.; Lee, D. H.; Park, I. H.; Bae, J. S.; Lee, T. W.; Kim, J.-Y.; Park, J. H.; Cho, Y. C.; Cho, C. R.; Jeong, S.-Y. Cu Mesh for Flexible Transparent Conductive Electrodes. *Sci. Rep.* **2015**, *5*, 10715.

(18) Khan, A.; Lee, S.; Jang, T.; Xiong, Z.; Zhang, C.; Tang, J.; Guo, L. J.; Li, W.-D. High-Performance Flexible Transparent Electrode with an Embedded Metal Mesh Fabricated by Cost-Effective Solution Process. *Small* **2016**, *12*, 3021−3030.

(19) Sakamoto, K.; Kuwae, H.; Kobayashi, N.; Nobori, A.; Shoji, S.; Mizuno, J. Highly Flexible Transparent Electrodes Based on Mesh-Patterned Rigid Indium Tin Oxide. *Sci. Rep.* **2018**, *8*, 2825.

(20) Manikandan, A.; Lee, L.; Wang, Y.-C.; Chen, C.-W.; Chen, Y.-Z.; Medina, H.; Tseng, J.-Y.; Wang, Z. M.; Chueh, Y.-L. Graphene-Coated Copper Nanowire Networks as a Highly Stable Transparent Electrode in Harsh Environments Toward Efficient Electrocatalytic Hydrogen Evolution Reactions. *J. Mater. Chem. A* **2017**, *5*, 13320−13328.

(21) Kim, Y. C.; Lee, S. J.; Jung, H.; Park, B.-E.; Kim, H.; Lee, W.; Myoung, J.-M. Optimization and Device Application Potential of Oxide−Metal−Oxide Transparent Electrode Structure. *RSC Adv.* **2015**, *5*, 65094−65099.

(22) Leijtens, T.; Eperon, G. E.; Pathak, S.; Abate, A.; Lee, M. M.; Snaith, H. J. Overcoming Ultraviolet Light Instability of Sensitized TiO_2 with Meso-Superstructured Organometal Tri-Halide Perovskite Solar Cells. *Nat. Commun.* **2013**, *4*, 2885.

(23) Im, H.-G.; Jeong, S.; Jin, J.; Lee, J.; Youn, D.-Y.; Koo, W.-T.; Kang, S.-B.; Kim, H.-J.; Jang, J.; Lee, D.; Kim, H.-K.; Kim, I.-D.; Lee, J.-Y.; Bae, B.-S. Hybrid Crystalline-ITO/metal Nanowire Mesh Transparent Electrodes and Their Application for Highly Flexible Perovskite Solar Cells. *NPG Asia Mater.* **2016**, *8*, e282.

(24) Shi, H.; Liu, C.; Jiang, Q.; Xu, J. Effective Approaches to Improve the Electrical Conductivity of PEDOT:PSS: A Review. *Adv. Electron. Mater.* **2015**, *1*, 1500017.

(25) Song, W.; Fan, X.; Xu, B.; Yan, F.; Cui, H.; Wei, Q.; Peng, R.; Hong, L.; Huang, J.; Ge, Z. All-Solution-Processed Metal-Oxide-Free Flexible Organic Solar Cells with Over 10% Efficiency. *Adv. Mater.* **2018**, *30*, 1800075.

(26) Fan, X.; Xu, B.; Liu, S.; Cui, C.; Wang, J.; Yan, F. Transfer-Printed PEDOT:PSS Electrodes Using Mild Acids for High Conductivity and Improved Stability with Application to Flexible Organic Solar Cells. *ACS Appl. Mater. Interfaces* **2016**, *8*, 14029−14036.

(27) Fan, X.; Wang, J.; Wang, H.; Liu, X.; Wang, H. Bendable ITO-Free Organic Solar Cells with Highly Conductive and Flexible PEDOT:PSS Electrodes on Plastic Substrates. *ACS Appl. Mater. Interfaces* **2015**, *7*, 16287−16295.

(28) Kim, Y. H.; Sachse, C.; Machala, M. L.; May, C.; Müller-Meskamp, L.; Leo, K. Highly Conductive PEDOT:PSS Electrode with Optimized Solvent and Thermal Post-Treatment for ITO-Free Organic Solar Cells. *Adv. Funct. Mater.* **2011**, *21*, 1076−1081.

(29) Vitoratos, E.; Sakkopoulos, S.; Dalas, E.; Paliatsas, N.; Karageorgopoulos, D.; Petraki, F.; Kennou, S.; Choulis, S. Thermal

DOI: 10.1021/acsami.8b10190
ACS Appl. Mater. Interfaces XXXX, XXX, XXX−XXX

Degradation Mechanisms of PEDOT:PSS. *Org. Electron.* **2009**, *10*, 61−66.
(30) Sun, X. J.; Wang, C. C.; Zhang, J.; Liu, G.; Zhang, G. J.; Ding, X. D.; Zhang, G. P.; Sun, J. Thickness Dependent Fatigue Life at Microcrack Nucleation for Metal Thin Films on Flexible Substrates. *J. Phys. D: Appl. Phys.* **2008**, *41*, 195404.
(31) Byoung-Joon, K.; Hae, A. S. S.; In-Suk, C.; Young-Chang, J. Electrical Failure and Famage Analysis of Multi-Layer Metal Films on Flexible Substrate During Cyclic Bending Deformation. *18th IEEE International Symposium on the Physical and Failure Analysis of Integrated Circuits (IPFA)*, July 4−7, 2011; pp 1−4.
(32) Poorkazem, K.; Liu, D.; Kelly, T. L. Fatigue Resistance of a Flexible, Efficient, and Metal Oxide-Free Perovskite Solar Cell. *J. Mater. Chem. A* **2015**, *3*, 9241−9248.
(33) Jin, W.-Y.; Ginting, R. T.; Ko, K.-J.; Kang, J.-W. Ultra-Smooth, Fully Solution-Processed Large-Area Transparent Conducting Electrodes for Organic Devices. *Sci. Rep.* **2016**, *6*, 36475.
(34) Jeong, S. H.; Yoon, K. H.; Min, B. G.; Lee, Y. S.; Lee, S. P.; Park, S. B. Heat resistance, Impact Strength, and Transparency of PET Copolymer Containing Fluorenylidene Bis(2-Phenoxyethanol). *Fibers Polym.* **2017**, *18*, 1638−1643.
(35) Davis, K. A.; Luo, X.; Mather, P. T.; Henderson, J. H. Shape Memory Polymers for Active Cell Culture. *J. Visualized Exp.* **2011**, *4*, e2903.
(36) Kim, Y.; Ryu, T. I.; Ok, K.-H.; Kwak, M.-G.; Park, S.; Park, N.-G.; Han, C. J.; Kim, B. S.; Ko, M. J.; Son, H. J.; Kim, J.-W. Inverted Layer-By-Layer Fabrication of an Ultraflexible and Transparent Ag Nanowire/Conductive Polymer Composite Electrode for Use in High-Performance Organic Solar Cells. *Adv. Funct. Mater.* **2015**, *25*, 4580−4589.
(37) Singh, A.; Dressick, W. J.; Lee, Y. Catalytic Enzyme-Modified Textiles for Active Protection from Toxins. U.S. Patent 20,070,014,838 A1, 2007.
(38) Jeon, N. J.; Noh, J. H.; Yang, W. S.; Kim, Y. C.; Ryu, S.; Seo, J.; Seok, S. I. Compositional Engineering of Perovskite Materials for High-Performance Solar Cells. *Nature* **2015**, *517*, 476−480.
(39) Bade, S. G. R.; Shan, X.; Hoang, P. T.; Li, J.; Geske, T.; Cai, L.; Pei, Q.; Wang, C.; Yu, Z. Stretchable Light-Emitting Diodes with Organometal-Halide-Perovskite-Polymer Composite Emitters. *Adv. Mater.* **2017**, *29*, 1607053.
(40) Vandeparre, H.; Liu, Q.; Minev, I. R.; Suo, Z.; Lacour, S. P. Localization of Folds and Cracks in Thin Metal Films Coated on Flexible Elastomer Foams. *Adv. Mater.* **2013**, *25*, 3117−3121.
(41) Bong, S.; Yeo, H.; Goh, M.; Ku, B.-C.; Kim, Y. Y.; Bong, P.-H.; Park, B.; You, N.-H. Synthesis and Characterization of Colorless Polyimides Derived from 4-(4-Aminophenoxy)-2,6-Dimethylaniline. *Macromol. Res.* **2016**, *24*, 1091−1097.
(42) Liang, C.; Wu, Z.; Li, P.; Fan, J.; Zhang, Y.; Shao, G. Chemical bath deposited rutile TiO 2 compact layer toward efficient planar heterojunction perovskite solar cells. *Appl. Surf. Sci.* **2017**, *391*, 337−344.
(43) Yella, A.; Heiniger, L.-P.; Gao, P.; Nazeeruddin, M. K.; Grätzel, M. Nanocrystalline Rutile Electron Extraction Layer Enables Low-Temperature Solution Processed Perovskite Photovoltaics with 13.7% Efficiency. *Nano Lett.* **2014**, *14*, 2591−2596.
(44) Wang, L.; Yuan, Z.; Egerton, T. A. Comparison of nano-particulate TiO2 prepared from titanium tetrachloride and titanium tetraisopropoxide. *Mater. Chem. Phys.* **2012**, *133*, 304−310.
(45) Ke, W.; Fang, G.; Liu, Q.; Xiong, L.; Qin, P.; Tao, H.; Wang, J.; Lei, H.; Li, B.; Wan, J.; Yang, G.; Yan, Y. Low-Temperature Solution-Processed Tin Oxide as an Alternative Electron Transporting Layer for Efficient Perovskite Solar Cells. *J. Am. Chem. Soc.* **2015**, *137*, 6730−6733.
(46) Lee, Y.; Paek, S.; Cho, K. T.; Oveisi, E.; Gao, P.; Lee, S.; Park, J.-S.; Zhang, Y.; Humphry-Baker, R.; Asiri, A. M.; Nazeeruddin, M. K. Enhanced Charge Collection with Passivation of the Tin Oxide Layer in Planar Perovskite Solar Cells. *J. Mater. Chem. A* **2017**, *5*, 12729−12734.
(47) Huang, X.; Hu, Z.; Xu, J.; Wang, P.; Wang, L.; Zhang, J.; Zhu, Y. Low-temperature processed SnO 2 compact layer by incorporating TiO 2 layer toward efficient planar heterojunction perovskite solar cells. *Sol. Energy Mater. Sol. Cells* **2017**, *164*, 87−92.
(48) Abdalla, J. T.; Huang, Y.-W.; Yu, Q.-J.; Wang, J.-Z.; Wang, J.-N.; Yu, C.-L.; Gao, S.-Y.; Jiao, S.-J.; Wang, D.-B.; Alarabi, A. M.; Abdellah, A. TiCl4 surface-treated SnO2 photoanodes for self-powered UV photodetectors and dye-sensitized solar cells. *Mater. Technol.* **2017**, *32*, 443−450.
(49) Zhou, Y.; Fuentes-Hernandez, C.; Shim, J.; Meyer, J.; Giordano, A. J.; Li, H.; Winget, P.; Papadopoulos, T.; Cheun, H.; Kim, J.; Fenoll, M.; Dindar, A.; Haske, W.; Najafabadi, E.; Khan, T. M.; Sojoudi, H.; Barlow, S.; Graham, S.; Bredas, J.-L.; Marder, S. R.; Kahn, A.; Kippelen, B. A Universal Method to Produce Low-Work Function Electrodes for Organic Electronics. *Science* **2012**, *336*, 327−332.
(50) Haynes, W. M.; Lide, D. R.; Bruno, T. J. *CRC Handbook of Chemistry and Physics*, 97th ed.; CRC Press: Boca Raton, FL, 2017.
(51) *Metals Handbook Ninth Edition Volume 13. Corrosion*; ASM International, 1987; p 1690.
(52) Revie, R.W. *Uhlig's Corrosion Handbook*, 3rd ed, 2011; p 850.
(53) Burleigh, T. D.; Ruhe, C.; Forsyth, J. Photo-Corrosion of Different Metals during Long-Term Exposure to Ultraviolet Light. *Corrosion* **2003**, *59*, 774−779.
(54) Bodner, J. J. *Dissolution of Titanium in Hydrochloric Acid*; The Degree of Master of Applied Science University of Windsor, 1964.
(55) Atkins, P. W.; De Paula, J. *Atkins' Physical Chemistry* 9th ed.; Oxford University Press: Oxford ; New York, 2010; p 928.
(56) Jeon, N. J.; Noh, J. H.; Kim, Y. C.; Yang, W. S.; Ryu, S.; Seok, S. I. Solvent engineering for high-performance inorganic−organic hybrid perovskite solar cells. *Nat. Mater.* **2014**, *13*, 897−903.
(57) Han, G. S.; Lee, S.; Duff, M. L.; Qin, F.; Lee, J.-K. Highly Bendable Flexible Perovskite Solar Cells on a Nanoscale Surface Oxide Layer of Titanium Metal Plates. *ACS Appl. Mater. Interfaces* **2018**, *10*, 4697−4704.

DOI: 10.1021/acsami.8b10190
ACS Appl. Mater. Interfaces XXXX, XXX, XXX−XXX